Algebraic Quantification of the Contribution of Active Regions to the Sun's Dipole Moment: Applications to Polar Field Estimates and Solar Cycle Forecasting

Shaonwita Pal,[1⋆] and Dibyendu Nandy[1,2 †]
[1]Center of Excellence in Space Sciences India, Indian Institute of Science Education and Research Kolkata, Mohanpur, West Bengal, India
[2]Department of Physical Sciences, Indian Institute of Science Education and Research Kolkata, Mohanpur, West Bengal, India

Accepted XXX. Received YYY; in original form ZZZ

ABSTRACT

The solar cycle is generated by a magnetohydrodynamic dynamo mechanism, which involves the induction and recycling of the toroidal and poloidal components of the Sun's magnetic field. Recent observations indicate that the Babcock-Leighton mechanism – mediated via the emergence and evolution of tilted bipolar active regions – is the primary contributor to the Sun's large-scale dipolar field. Surface flux transport models and dynamo models have been employed to simulate this mechanism, which also allows for physics-based solar cycle forecasts. Recently, an alternative analytic method has been proposed to quantify the contribution of individual active regions to the Sun's dipole moment. Utilizing solar cycle observations spanning a century, here we test the efficacy of this algebraic approach. Our results demonstrate that the algebraic quantification approach is reasonably successful in estimating dipole moments at solar minima over the past century – providing an independent verification of the Babcock-Leighton mechanism as the primary contributor to the Sun's dipole field variations. We highlight that this algebraic methodology stands as an independent approach for estimating the dipole moment at the minima of solar cycles, relying on characteristics of the sunspot cycle. We also show how this method may be utilized for solar cycle predictions; our estimate of the Sun's dipole field at the end of cycle 24 using this approach indicates that solar cycle 25 would be a moderately weak cycle, ranging between solar cycle 20 and cycle 24.

Key words: Bipolar magnetic field – Solar cycle – Axial dipole moment – Babcock-Leighton mechanism – Cycle Prediction

1 INTRODUCTION

Our home star, the Sun, is a gigantic hot ball of plasma with inherent magnetic activity. Sunspots, strongly magnetized dark regions on the solar surface (Hale 1908), serve as reliable indicators of this magnetic activity. Observations show that sunspot numbers undergo periodic variations following an 11-year recurring cycle, known as the solar cycle (Clark & Stephenson 1978; Schwabe 1844; Schatten 2003; Hathaway 2015). Halfway through the solar cycle, the Sun's activity reaches its peak, or the solar maximum, with the highest number of sunspot emergences. During this maximum phase, its magnetic north and south poles flip, after which the Sun calms down until it reaches a solar minimum, indicating the beginning of a new sunspot cycle. During solar maximum, a more magnetically active Sun leads to frequent occurrences of magnetic outbursts and plasma outflows, such as solar flares and coronal mass ejections(CMEs). These phenomena significantly impact satellite operations, space-based technologies and the Earth's upper atmosphere (Kutiev, Ivan et al. 2013; Solanki 2002). Therefore, understanding the dynamics of the solar cycle is crucial to be able to predict the Sun's magnetic activity and its consequences on space weather and planetary environments (Petrovay 2020; Nandy 2021; Bhowmik et al. 2023; Nandy et al. 2023b).

The magnetic cycle of the Sun can be explained through the Babcock-Leighton (BL) Solar Dynamo theory, which primarily establishes the interplay between the global poloidal field and the toroidal field in the presence of various plasma flows within the solar convection zone (Wang et al. 1991; Leighton 1964; Charbonneau 2020). During the initial phase of the solar cycle, the global magnetic field is primarily dominated by the poloidal field component. The Sun's differential rotation stretches this poloidal field in the longitudinal direction, leading to the formation of the toroidal field in the tachocline region (Snodgrass 1987). Subsequently, these toroidal flux ropes are unstable within the convection zone, and due to magnetic buoyancy, they emerge on the solar surface as dark sunspots. Once the tilted bipolar active regions (BMRs) appear on the solar surface, their evolution and the regeneration of the toroidal field are primarily governed by the Babcock-Leighton (BL) mechanism (Babcock 1961). The BL mechanism constitutes two processes: one is the annihilation of the leading polarities across two hemispheres, and the second one is the drift and diffusion of the following polarity towards the pole. These unipolar magnetic regions cancel the existing poloidal field at the pole and generate the poloidal field with opposite signs for the new solar cycle. Altogether, the BL-type Solar Dynamo model effectively captures the key aspects of the decay

⋆ shao.physics@gmail.com
† E-mail: dnandi@iiserkol.ac.in

and dispersal of sunspots, polar field reversal, and the new polar field buildup (Charbonneau 2007; Kitchatinov & Olemskoy 2011; Cameron & Schüssler 2017; Bhowmik & Nandy 2018; Kumar et al. 2019; Pal et al. 2023).

It is well-established that during a solar activity minimum, the poloidal magnetic field, often referred to as polar field, and other polar field proxies (for example, axial dipole moment, open heliospheric magnetic flux, A-t index, etc.) strongly correlates with the amplitude of the succeeding cycle (Schatten et al. 1978; Yeates et al. 2008; Muñoz-Jaramillo et al. 2012). Utilizing polar field proxies as a seed for predicting the amplitude of the next solar cycle is known as the 'precursor method', which has evolved as one of the most successful techniques of sunspot cycle prediction (Nandy 2021; Petrovay 2020). However, selecting an appropriate precursor for solar cycle forecasts relies on substantial physical insight and aids in accurate cycle predictions. In the context of the dynamo mechanism, the dipole moment (DM) closely relates to the poloidal field at the end of a solar cycle. Analysis of the observed photospheric magnetic field over the past four solar cycles suggests that the reversal of the dipole moment epoch aligns better with the cycle maximum than the average timing of polar field reversal (Upton & Hathaway 2013; Iijima et al. 2017; Virtanen et al. 2019). Moreover, the dipole moment contains information from the entire photosphere, mitigating the effects of a hemispherically asymmetric magnetic field distribution. Hence, during the solar minimum, the axial dipole moment component acts as a seed for the toroidal component of the next cycle (Upton & Hathaway 2018; Charbonneau 2020; Nandy et al. 2023a).

Predicting the dipole moment at the end of the solar cycle minimum is a more feasible approach to estimate the strength of the next cycle. This task can be achieved through various methods, including observations and physics-based numerical models (Upton & Hathaway 2013; Virtanen et al. 2019; Jaswal et al. 2023). However, determining the dipole moment through magnetogram analysis is limited to a few past solar cycles and thus relies on physical models such as the flux transport dynamo model. One commonly used physics-based model for predicting the dipole moment is the Surface Flux Transport (SFT) model based on the BL mechanism (Upton & Hathaway 2013; Bhowmik & Nandy 2018; Pal et al. 2023; Yeates et al. 2023). However, calibrating such numerical models sometimes becomes challenging and time-consuming. What if we explore an alternative to numerical methods, moving away from complex computer-intensive modelling and adopting a simplified approach?

The first attempt in this direction was made by Jiang et al. (2019); Petrovay et al. (2020). They introduced a mathematical framework aimed at calculating the distinct contributions of each emerging active region that collectively generate the overall global dipole moment during the cycle minimum. In their work, synthetic sunspot time series were utilized to compute the ultimate dipole moment, and the results were compared with those derived from the 2 × 2D dynamo model (Lemerle & Charbonneau 2017) and simulations from the SFT model (Petrovay et al. 2020; Nagy et al. 2020; Wang et al. 2021; Pal et al. 2023). Subsequently, Pal et al. (2023) adopted a similar approach to investigate the impact of anomalous active regions, specifically the combinations of synthetic Anti-Hale and Anti-Joy regions, on the solar cycle.

In this study, we employ the modified analytical approach to calculate the ultimate dipole moment at the end of a solar cycle, using the observational properties of bipolar active regions emerging throughout the declining phase of the sunspot cycle. Initially, we validate our method by estimating the dipole moment at the minima of solar cycles 14 to 23 and comparing it with observations. Subsequently, based on the algebraically derived dipole moment for solar cycle 24, we predict the peak amplitude of the ongoing solar cycle, *i.e.* solar cycle 25, along with the associated uncertainties. We have also discussed the advantages and limitations of our methodology using observational insights.

2 METHODS

Here, we discuss the method of quantifying the ultimate axial dipole moment of a solar cycle mathematically, which was first adopted by Petrovay et al. (2020). A spatially two-dimensional Surface Flux Transport model can be simplified to an azimuthally averaged 1D SFT model (Petrovay et al. 2020; Pal et al. 2023). In this model, tilted sunspots transform into a bipolar flux ring with a finite latitudinal separation. Thus, the tilted sunspot can be considered as a magnetic dipole, with two opposite polarities separated by a finite distance. Now, the 'initial unsigned dipole moment' of any i^{th} active region can be expressed as,

$$\delta D_{1,i} = \frac{3}{4\pi R^2}\, \Phi_i \, d_{\lambda_i} \cos\lambda_i . \tag{1}$$

Here, λ_i is the latitudinal position, and d_{λ_i} denotes the latitudinal separation of the leading and following polarities of the i^{th} sunspot, Φ_i represents the magnetic flux content in the concerned sunspot.

The evolution of the dipole moment involves additional physical factors that govern the regular dipole moment reversal and its accumulation. The dipole moment build-up may be influenced by the radial diffusion of the photospheric magnetic field. This radial diffusion term is expressed as $\mathrm{e}^{-t/\tau}$, where τ represents the exponential decay term. This expression indicates that the dipole moment gradually diminishes over time due to the radial outflows.

Another asymptotic dependency of the dipole moment is linked to the latitudinal position of sunspots. Jiang et al. (2014) demonstrated, through SFT simulations, that the amplitude of the dipole moment decreases with increasing latitude. This asymptotic dipole moment contribution factor, denoted as f_∞, can be modeled as a Gaussian function of latitude: $f_\infty = \mathrm{C}\exp(-\lambda^2/2\lambda_R^2)$. Here, λ_R and C depend on the transport parameters specific to a given SFT model. These constants remain fixed for each solar cycle in our analysis, therefore removing the necessity to constrain them from the SFT model.

Thus, if an i^{th} active region emerges at time t_i, then the 'ultimate dipole moment' contribution at the end of 'cycle n' at time t_{n+1} becomes:

$$\delta D_{\mathrm{U},i} = f_{\infty,i}\, \delta D_{1,i}\, \mathrm{e}^{(t_i - t_{n+1})/\tau} . \tag{2}$$

The initial dipole moment contribution from i^{th} sunspot ($\delta D_{1,i}$) will be positive or negative depending on the polarity of the sunspot that is closest to the equator. We consider a positive contribution for Hale-Joy sunspots and a negative contribution for anomalous sunspots towards the ultimate dipole moment. In our recent study of anomalous active regions, we utilized this sign conversion of dipole moment, revealing that the dipole moment decreases at solar minima when multiple anomalous regions appear in a solar cycle (Pal et al. 2023).

According to the BL mechanism, the sunspots of the current cycle decay and disperse due to the plasma flows and cancel the old cycle's dipole moment. Hence, the dipole moment at the end of a solar cycle is the combined result of the cancellation of the preceding cycle's dipole moment and a generation of the new cycle's dipole moment. Here, we use this fact considering the active regions appearing after the reversal of the old cycle dipole moment polarity will contribute to building a new dipole moment (as DM is almost zero at reversal).

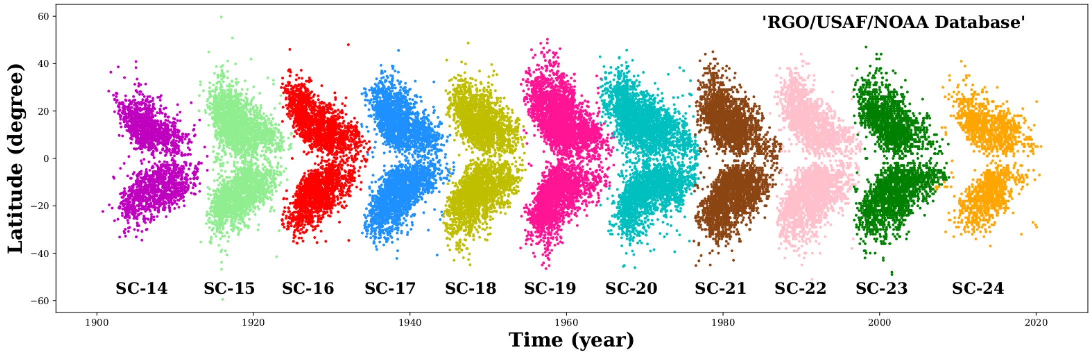

Figure 1. The butterfly diagram depicts the spatiotemporal changes spanning Solar Cycles 14 to 24. This figure illustrates the evolution of sunspots across the last 11 solar cycles, using time and latitudinal position data sourced from the RGO/USAF/NOAA Data Centre (2023). Distinct colours are used to differentiate between the various solar cycles.

Thus, the net input into the global dipole moment from all emerged active regions during the n^{th} cycle can be expressed as the sum of the dipole moment contributions from individual sunspots that appeared after reversal time. The calculation is as follows,

$$\begin{aligned}
\mathrm{DM}_{n+1} - \mathrm{DM}_n &= \Delta \mathrm{DM} \\
&= \sum_i \delta D_{\mathrm{U},i} \\
&= \sum_i f_{\infty,i}\, \delta D_{1,i}\, \mathrm{e}^{(t_i - t_{n+1})/\tau} \\
&= \frac{3}{4\pi R^2} \sum_i \Phi_i\, d_{\lambda_i} \cos\lambda_i \exp(-\lambda_i^2)\,. \quad (3)
\end{aligned}$$

Here, ‘i’ takes care of all active regions that emerged after time reversal. ΔDM denotes the dipole moment at the end of solar cycle n. We assume there are no radial outflows, *i.e.* τ is infinity.

We compute the dipole moment at solar cycle minima for solar cycles 14 to cycle 24, utilizing the observed characteristics of the sunspots and the observed time reversal epoch of the dipole moment. We use the dipole moment reversal timing epoch from the WSO average polar field, available only for solar cycle 21 to cycle 24 (WSO Data Centre 2023). For the rest of solar cycles (*i.e.* solar cycle 14 to cycle 20), we opt for the sunspot cycle peak time because the Sun’s global dipole magnetic field generally flips its polarity around the maximum phase of the solar cycle. We extract the solar cycle maximum epoch from SILSO World Data Center (2019) time series. Our analysis considers these dipole moment reversal timings as the standard reversal epoch.

We use the RGO/USAF/NOAA Data Centre (2023) to extract information on the latitudinal position and area of the bipolar active regions ranging from solar cycle 14 to cycle 24. In this study, we specifically focus on the statistics of active regions when they reach their maximum size. Figure 1 illustrates the butterfly diagram, spanning the last century, with time and latitude information obtained from the RGO/USAF/NOAA database.

3 RESULTS AND DISCUSSIONS

3.1 Dipole moment comparison for past solar cycles spanning a century.

Utilizing the observational sunspot characteristics in the aforementioned analytical model, we estimate the century-scale calibrated global axial dipole moment at each solar minimum, spanning from solar cycle 14 to cycle 23. These algebraically derived dipole moments can be compared with observational dipole moment proxies, considering that the Sun’s global magnetic field is primarily dipolar during the solar minimum. For this purpose, we use three observational time series: 1) Polar flux obtained from MWO polar faculae count (Muñoz-Jaramillo et al. 2012), 2) Makarov’s A-t index (Makarov et al. 2001), and 3) WSO polar field (WSO Data Centre 2023). We consider the average northern and southern hemispheric polar flux or polar field as a proxy for the dipole moment.

Our mathematical approach focuses on determining the dipole moment’s value at the end of the solar cycle rather than explaining its time evolution. Thus, we use the average polar field derived from the WSO Data Centre (2023) from 1976 onwards to calibrate the computed dipole moment. Accordingly, we scale the algebraically derived dipole moment corresponding to each minimum with the same constant factor, calibrated with the averaged polar field from the WSO polar field data source. In Figure 2, red stars denote the estimated calibrated dipole moment compared with MWO polar flux, Makarov’s A-t index and WSO polar field marked with magenta, green and orange. We calculate the potential error in the dipole moment computation by choosing the accurate dipole moment reversal time. The dipole moment reversal epoch may not always align with the solar cycle maxima; it can lead or lag the sunspot maximum epoch. If the dipole moment reversal timing lags the solar maximum epoch, then the total sunspots contribution towards the dipole moment will decrease, which in turn dampens the ultimate dipole moment. At the same time, the dipole moment will increase if the reversal time leads to the solar maximum epoch. Therefore, we assume that the dipole moment reversal time varies within a two-year interval around the standard reversal epoch, encompassing one year before and one year after the standard reversal epoch. Following that, we compute the contribution to the dipole moment at the endpoints of specified reversal time intervals. Based on this, we introduce an error bar on the derived dipole moment (see Figure 2). The algebraically derived dipole moments from solar cycle 14 to cycle 24 are tabulated in Table 1.

To check the efficacy of our methodology, we conduct a correlation analysis between the analytically calculated dipole moment and the observed polar field proxies at the solar minima. The results are depicted in Figure 3. The correlation analysis demonstrates a reasonably good match between the algebraically derived dipole moment and the observed data, with one notable exception - solar

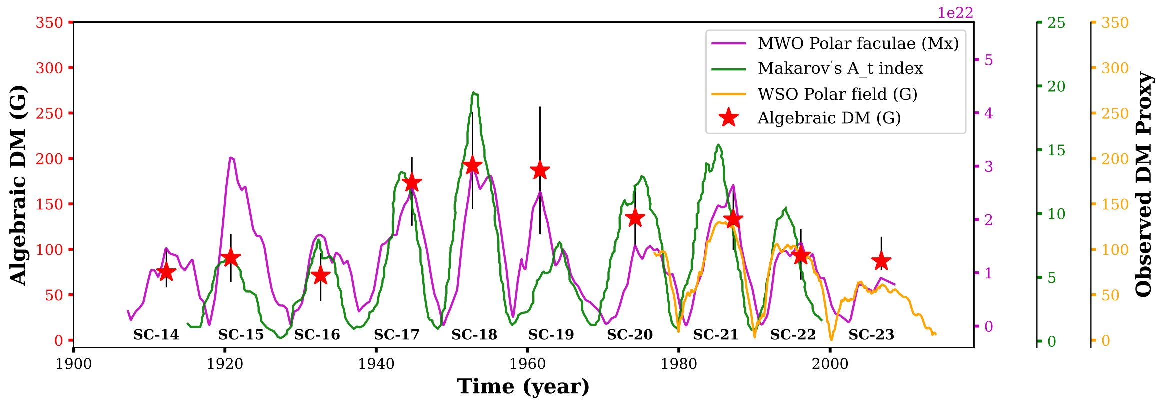

Figure 2. Time series of Dipole moment (DM) proxies ranging from solar cycle 14 to 24. In this representation, the MWO polar faculae data is depicted in magenta (Muñoz-Jaramillo et al. 2012), Makarov's A-t index (Makarov et al. 2001) is shown in green, and the WSO polar field data (WSO Data Centre 2023) is represented in orange. All polar field data is averaged from the northern and southern hemispheres to facilitate comparison with the dipole moment. Additionally, red stars indicate the algebraically computed ultimate dipole moment at the end of each cycle spanning solar cycle 14 to solar cycle 23.

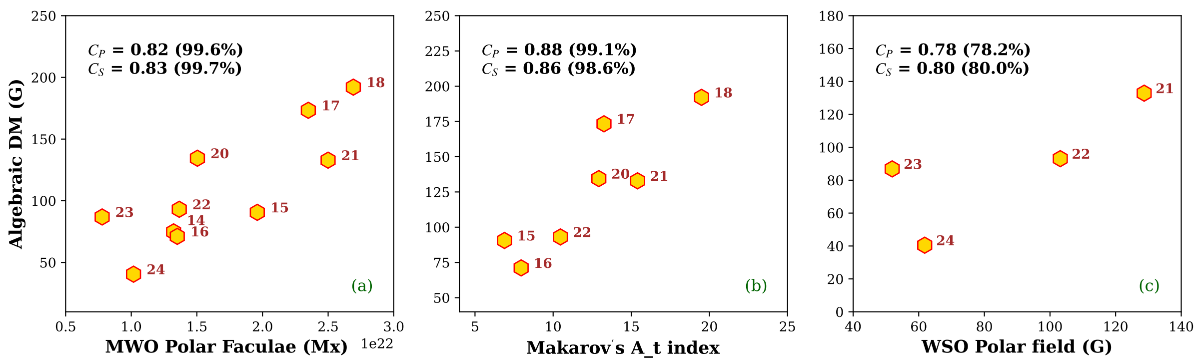

Figure 3. Statistical correlation analysis between observational dipole moment proxies and algebraic dipole moment. In Panel (a), (b), and (c), three different databases have been considered as the observed DM proxies: MWO polar faculae data (Muñoz-Jaramillo et al. 2012), Makarov's A-t index (Makarov et al. 2001), and WSO polar field (WSO Data Centre 2023).

cycle 19. The computed dipole moment for solar cycle 19, deviates significantly from the observational polar field proxies, as shown in panels a) and b) of Figure 3. Given this, we consider solar cycle 19 an outlier and exclude it from the correlation analysis.

After omitting solar cycle 19, we find a statistically significant correlation coefficient between the mathematically computed dipole moment and the observed polar field proxies, as mentioned in Figure 3. In Section 3.3, we discuss potential factors contributing to our inability to retrieve the ultimate dipole moment of solar cycle 19. This study reveals that the analytically estimated dipole moment for the past ten solar cycles aligns with the observed polar flux. This alignment underscores the physics of decay and dispersal of sunspots, contributing to the ultimate build-up of the dipole moment from a mathematical perspective.

3.2 Prediction of solar cycle 25.

In this study, we find a significant deviation in the dipole moment of sunspot cycle 19. This deviation influences the peak amplitude of solar cycle 20, given the causal connection between the dipole mpoment at the solar minimum and the subsequent solar cycle strength. Hence, we exclude the dipole moment of solar cycle 19 and the peak amplitude of sunspot cycle 20 from our current analysis.

We integrate the SIDC SILSO yearly averaged sunspot numbers dataset (SILSO World Data Center 2019) into our analysis to empirically predict ongoing solar cycle 25. First, we perform a correlation analysis between the analytically derived dipole moment at the end of a cycle and the averaged sunspot number of the consequent cycle. The scatter plot in Figure 4 illustrates a strong positive correlation (with 99% confidence level) between these two quantities. This correlation suggests a potential empirical avenue for forecasting future cycles. Also, for the first time, we reconstruct the dipole moment spanning a century (from 1902 onwards) and utilize it for solar cycle prediction.

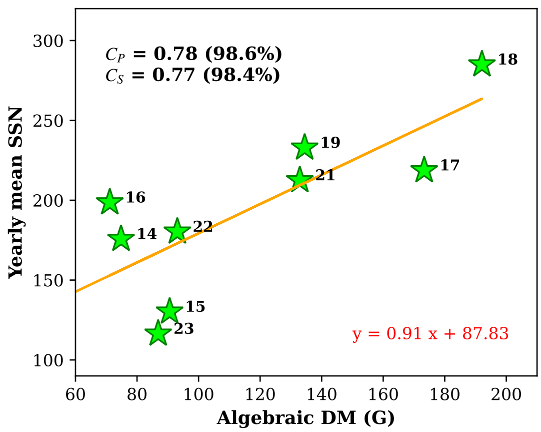

Figure 4. Statistical correlation analysis between analytically computed dipole moment (D) and the yearly averaged sunspot number (N) obtained from SILSO World Data Center (2019). The scattered data points have been fitted with a linear regression model, visually represented by the yellow line. The established relationship is expressed as follows: N = 0.91 × D + 87.83.

Table 1. Analytically derived dipole moment (DM) at the end of the solar cycle and predicted sunspot numbers, spanning last century (from solar cycle 14 to cycle 25).

Solar cycle #	DM at solar minima (G)	Peak sunspot #
SC-14	74.80 [+26,-17]	-
SC-15	90.60 [±26]	156 [+25,-20]
SC-16	71.14 [+25,-28]	171 [+28,-22]
SC-17	173.32 [+28,-47]	153 [+24,-19]
SC-18	192.08 [+59,-47]	246 [+42,-32]
SC-19	186.79 [±70]	264 [+46,-35]
SC-20	134.47 [+34,-32]	259 [+45,-34]
SC-21	132.89 [+33,-34]	211 [+35,-34]
SC-22	93.09 [+29,-26]	209 [+35,-27]
SC-23	86.87 [+27,-9]	173 [+28,-22]
SC-24	40.48 [+20,-15]	167 [+27,-22]
SC-25	-	125 [+19,-16]

We fit this scatter plot in Figure 4 with a linear regression model and find a relationship between the analytically derived dipole moment (D) and the sunspot number (N). The relationship is: N = 0.91 × D + 87.83. Utilizing the ultimate analytic dipole moment at solar minimum (D), we calculate the yearly average sunspot number (N) for solar cycle 14 to solar cycle 24. This method effectively reconstructs the past cycles, except solar cycle 20. Figure 5 shows that the empirically derived sunspot number at solar cycle maxima (red stars) is overplotted with the SIDC/SILSO sunspot numbers. This result is also tabulated in Table 1. The deviation in cycle 20 is understandable, as our inability to accurately determine the cycle 19 dipole moment affects the subsequent cycle.

Finally, by inputting the analytically computed ultimate dipole moment for solar cycle 24 into our fitted linear relationship, our prediction suggests that solar cycle 25 will be stronger than its predecessor, solar cycle 24. To be precise, we anticipate that solar cycle 25 will reach a yearly average peak sunspot number of 125, ranging between solar cycle 20 and cycle 24 (see Figure 5). The reasonably good match of derived sunspot cycle maxima with the observed sunspot number over the last centuries also suggests that the dipole moment precursor is a promising candidate for solar cycle forecasts.

3.3 Dependency of Algebraic Method on bipolar active region (BMR) characteristics.

In this analytic model, the dipole moment at the solar cycle minima depends on the quantity and flux content of active regions that emerge after the reversal of dipole moment polarity. To verify the existence of this signature in the observation, we conduct a correlation analysis between the total number of active regions that appeared after the time reversal and the observational or algebraic dipole moment at the end of the sunspot cycle. We find a high correlation coefficient between the total number of active regions and the ultimate algebraic dipole moment (Pearson coefficient 0.93 with 99.9% confidence level). This result is depicted in panel (b) of Figure 6. Our finding indicates that as the number of sunspots increases, there is a corresponding rise in the ultimate dipole moment. However, this relationship is not consistently observed in practice. Pearson coefficient suddenly drops to 0.47 (83.3%) if we replace the algebraic dipole moment with the observational polar flux (see Panel (a) in Figure 6). Particularly during solar cycle 19, the highest number of sunspots appeared, but its dipole moment at the end of the cycle was surprisingly small, as illustrated in the observation (see Panel (a) in Figure 6).

Similarly, we observe a strong linear correlation of 0.98 (99.9%) between the total flux content of the sunspots emerging after dipole moment reversal and the ultimate algebraic dipole moment, as depicted in Panel (d) of Figure 6. Nevertheless, the correlation analysis of Panel (c) presents a weak relationship (with a linear correlation of 0.55, 90.3%) between the flux content of the sunspots and the observed average polar flux at cycle minima. Hence, the observed polar flux amplitude's dependency on the total flux content in emerged sunspots is not evident for all solar cycles in the observational polar faculae data (see Panel (c) in Figure 6).

The strong correlation between the number of sunspots and their magnetic flux content can significantly impact our algebraic calculations, occasionally yielding a dipole moment value much higher than expected. Due to this fact, we are unable to estimate the ultimate dipole moment of solar cycle 19 using algebraic techniques. Consequently, we cannot predict the yearly averaged sunspot number for solar cycle 20.

Our analysis suggests that variations in BMR properties are not the sole factors contributing to the irregularities observed in the solar cycle. Other sources, such as the nonlinear effects arising from the feedback of plasma flows, fluctuations in meridional flows across cycles, plasma inflows, and other stochastic processes, also play a significant role in accounting for the variability observed in the buildup of the ultimate dipole moment and, consequently, in shaping the solar cycle. Integrating these nonlinear effects into the currently simplified algebraic technique can enhance the accuracy of dipole moment calculations and subsequently improve the forecasting of solar cycles.

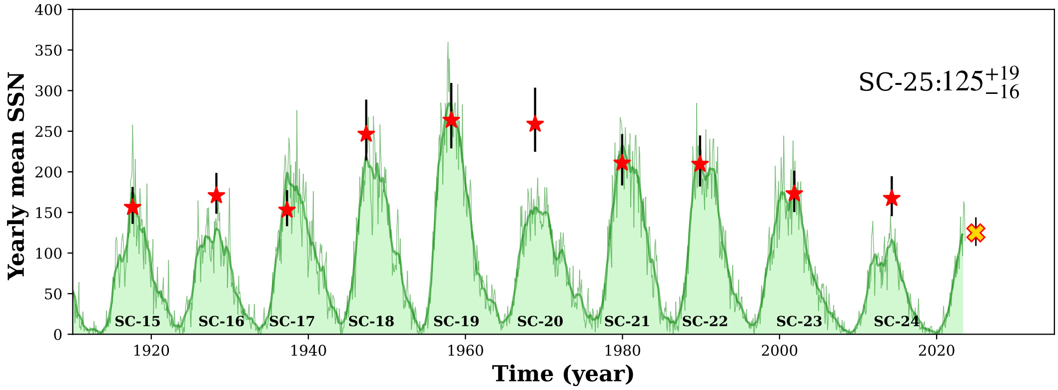

Figure 5. Solar Cycle 25 Prediction. The peak sunspot number for the last ten cycles is calculated and depicted as red stars. This is overlaid with the yearly averaged sunspot number time-series from SILSO World Data Center (2019). Utilizing the ultimate dipole moment of cycle 24, the predicted amplitude of solar cycle 25 is 125^{+19}_{-16}, denoted by the yellow cross.

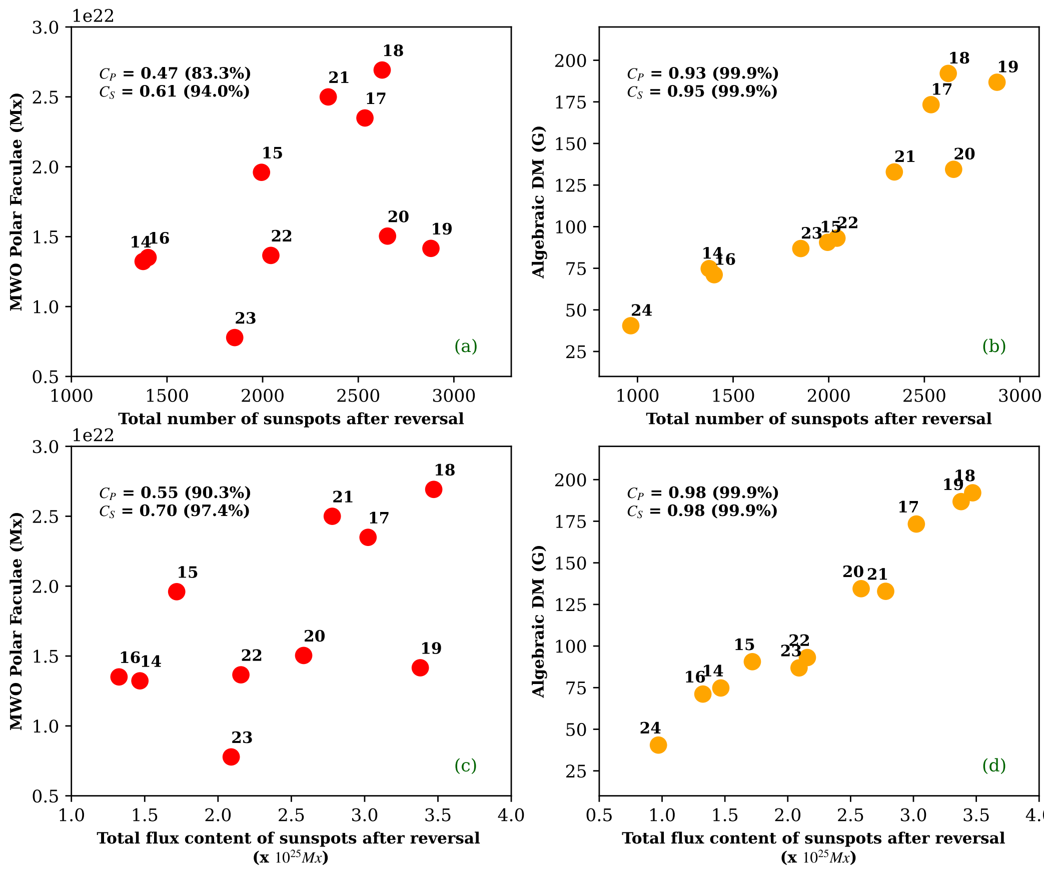

Figure 6. The correlation between the algebraic dipole moment (DM) and various properties of the Bipolar Magnetic Regions (BMRs). In Panels (a) and (b), the correlation is observed between the total number of sunspots appearing after the dipole moment reversal and the observational average polar flux (Panel (a)) and algebraic dipole moment (Panel (b)). Similarly, panels (c) and (d) illustrate the correlation between the total flux content of all sunspots emerging after the reversal of the dipole moment and the observational average polar (Panel (c)) and algebraic dipole moment (Panel (d)).

4 CONCLUSION

In summary, we employ a simplified analytic technique, following the approach by Petrovay et al. (2020), to calculate the Sun's dipole moment at the solar minimum. We assess the effectiveness of algebraically derived dipole moment by comparing it with diverse observational data sets from solar cycle 14 to solar cycle 23. We find that this analytic method reasonably estimates the dipole moment of solar cycles in observation spanning a century. However, solar cycle 19 is an exception, being the strongest and most extreme cycle in the observation.

We obtain a strong relationship between the dipole moment of the preceding cycle and the sunspot number of the subsequent solar cycle. Using this empirical relationship, we compute the yearly averaged sunspot number from solar cycle 14 to cycle 24. These estimates match the observations well. This is taken advantage of to predict the peak amplitude of sunspot cycle 25. We utilize the algebraically derived dipole moment of solar cycle 24 as a precursor to forecast the strength of solar cycle 25. The predicted amplitude is 125, with a range which places cycle 25 between sunspot cycle 20 and cycle 24. For the first time, we estimate the dipole moment at solar minimum spanning a century, allowing a robust test of its value as a precursor for predicting solar cycle amplitudes.

Our work provides strong support to the idea that the emergence and evolution of tilted bipolar sunspot pairs are the primary contributors to the Sun's dipole field – the so-called Babcock-Leighton mechanism. The surface flux transport models rely on these ideas, and Numerous dynamo models have been developed in recent times, which reproduce diverse characteristics of the sunspot cycles. (Hazra & Nandy 2016, 2019; Saha et al. 2022; Pal et al. 2023)

This analytic method for estimating the Sun's dipole moment relies on diverse properties of sunspots, including their latitudinal position, flux content, separation between two polarities and the total number of active regions that appear in a solar cycle. This method's dependency on BMR characteristics can sometimes lead to deviation from observations in the theoretical dipole moment calculation. For example, in our analysis, we observe a deviation in the dipole moment of solar cycle 19, which in turn impacts the reconstructed amplitude of solar cycle 20. This occurs because the direct dependency on the total number of sunspots and the flux content can weaken the accuracy of dipole moment estimates at the end of the cycle, which is not always seen in the observation. Nevertheless, such deviations are not always significant, and the dipole moment at solar minima derived from this analytic method closely matches the observational proxy based on polar flux. Notably, the sunspot amplitudes of past cycles empirically derived from the analytically estimated dipole moment match sunspot cycle amplitudes spanning the last century. Taken together, these corroborate our algebraic approach for dipole moment estimations.

We emphasize that our methodology is an independent means to estimate the dipole moment at the minima of solar cycles based on characteristics of the sunspot time series. Therefore, this provides a straightforward theoretical tool to reconstruct the dipole moment at the minima of past sunspot cycles. We note that our methodology is not dependent on any model parameters or parametrization of transport processes as done in surface flux transport models.

There are certain shortcomings in such an approach, which relies on a 1D linear model. For example, details study of inter-active region interections, exploration of non-axisymmetric phenomenon and influence of non-linearities can not be addressed. For the latter, one must still rely on numerical simulations of spatially extended time-dependent magnetic field evolution models. However, when it comes to estimating the solar dipole moment and making predictions for the solar cycle, the algebraic method explored here appears to be a powerful tool.

5 ACKNOWLEDGEMENT

This research is conducted at the Center of Excellence in Space Sciences India (CESSI), supported by IISER Kolkata and the Ministry of Education, Government of India. We acknowledge insightful discussions with Kristof Petrovay regarding this work. We are also thankful to the members of the ISSI team entitled "What Determines The Dynamo Effectivity Of Solar Active Regions?" (supported by the International Space Science Institute in Bern, Switzerland) for helpful discussions.

6 DATA AVAILABILITY

We utilize the yearly and monthly averaged sunspot numbers from World Data Center SILSO, Royal Observatory of Belgium, Brussels (SILSO World Data Center 2019). The dipole moment proxies are sourced from various datasets, including MWO polar faculae data (Muñoz-Jaramillo et al. 2012), Makarov's dipole-octupole index or A-t index (Makarov et al. 2001), and WSO polar field data (WSO Data Centre 2023). Additionally, we extract Bipolar Magnetic Region (BMR) properties from the Royal Greenwich Observatory/USAF-NOAA active region database compiled by David H. Hathaway (RGO/USAF/NOAA Data Centre 2023). The century-scale algebraically derived dipole moment data and solar cycle 25 prediction data will be made accessible upon reasonable requests.

REFERENCES

Babcock H. W., 1961, ApJ, 133, 572
Bhowmik P., Nandy D., 2018, Nature Communications, 9, 5209
Bhowmik P., Jiang J., Upton L., Lemerle A., Nandy D., 2023, arXiv e-prints, p. arXiv:2303.12648
Cameron R. H., Schüssler M., 2017, A&A, 599, A52
Charbonneau P., 2007, Advances in Space Research, 39, 1661
Charbonneau P., 2020, Living Reviews in Solar Physics, 17, 4
Clark D. H., Stephenson F. R., 1978, QJRAS, 19, 387
Hale G. E., 1908, ApJ, 28, 315
Hathaway D. H., 2015, Living Reviews in Solar Physics, 12, 4
Hazra S., Nandy D., 2016, ApJ, 832, 9
Hazra S., Nandy D., 2019, MNRAS, 489, 4329
Iijima H., Hotta H., Imada S., Kusano K., Shiota D., 2017, A&A, 607, L2
Jaswal P., Saha C., Nandy D., 2023, arXiv e-prints, p. arXiv:2307.00520
Jiang J., Cameron R. H., Schüssler M., 2014, ApJ, 791, 5
Jiang J., Song Q., Wang J.-X., Baranyi T., 2019, ApJ, 871, 16
Kitchatinov L. L., Olemskoy S. V., 2011, Astronomy Letters, 37, 656
Kumar R., Jouve L., Nandy D., 2019, A&A, 623, A54
Kutiev, Ivan et al., 2013, J. Space Weather Space Clim., 3, A06
Leighton R. B., 1964, ApJ, 140, 1547
Lemerle A., Charbonneau P., 2017, ApJ, 834, 133
Makarov V. I., Tlatov A. G., Callebaut D. K., Obridko V. N., Shelting B. D., 2001, Sol. Phys., 198, 409
Muñoz-Jaramillo A., Sheeley N. R., Zhang J., DeLuca E. E., 2012, ApJ, 753, 146
Nagy M., Petrovay K., Lemerle A., Charbonneau P., 2020, Journal of Space Weather and Space Climate, 10, 46
Nandy D., 2021, Sol. Phys., 296, 54
Nandy D., et al., 2023a, Exploring the Solar Poles: The Last Great Frontier of the Sun, doi:10.48550/ARXIV.2301.00010, `https://arxiv.org/abs/2301.00010`

Nandy D., et al., 2023b, Journal of Atmospheric and Solar-Terrestrial Physics, 248, 106081
Pal S., Bhowmik P., Mahajan S. S., Nandy D., 2023, ApJ, 953, 51
Petrovay K., 2020, Living Reviews in Solar Physics, 17, 2
Petrovay K., Nagy M., Yeates A. R., 2020, Journal of Space Weather and Space Climate, 10, 50
RGO/USAF/NOAA Data Centre 1874-2023, `https://solarscience.msfc.nasa.gov/greenwch.shtml`
SILSO World Data Center 1700-2019, `http://www.sidc.be/silso/`
Saha C., Chandra S., Nandy D., 2022, Monthly Notices of the Royal Astronomical Society: Letters, 517, L36
Schatten K., 2003, Advances in Space Research, 32, 451
Schatten K. H., Scherrer P. H., Svalgaard L., Wilcox J. M., 1978, Geophys. Res. Lett., 5, 411
Schwabe H., 1844, Astronomische Nachrichten, 21, 233
Snodgrass H. B., 1987, Sol. Phys., 110, 35
Solanki S. K., 2002, Astronomy & Geophysics, 43, 5.9
Upton L., Hathaway D. H., 2013, The Astrophysical Journal, 780, 5
Upton L. A., Hathaway D. H., 2018, Geophys. Res. Lett., 45, 8091
Virtanen I. O. I., Virtanen I. I., Pevtsov A. A., Mursula K., 2019, A&A, 632, A39
WSO Data Centre 1976-2023, `http://wso.stanford.edu/Polar.html`
Wang Y. M., Sheeley N. R. J., Nash A. G., 1991, ApJ, 383, 431
Wang Z.-F., Jiang J., Wang J.-X., 2021, A&A, 650, A87
Yeates A. R., Nandy D., Mackay D. H., 2008, ApJ, 673, 544
Yeates A. R., Cheung M. C. M., Jiang J., Petrovay K., Wang Y.-M., 2023, Space Sci. Rev., 219, 31

This paper has been typeset from a TEX/LATEX file prepared by the author.